

Urban Heat Island Modeling in Conjunction with Satellite-Derived Surface/Soil Parameters

JAN HAFNER AND STANLEY Q. KIDDER

Cooperative Institute for Research in the Atmosphere, Colorado State University, Fort Collins, Colorado

(Manuscript received 31 May 1997, in final form 15 June 1998)

ABSTRACT

Although it has been studied for over 160 years, the urban heat island (UHI) effect is still not completely understood, yet it is increasingly important. The main purpose of this work is to improve UHI modeling by using AVHRR (Advanced Very High Resolution Radiometer) satellite data to retrieve the surface parameters (albedo, as well as soil thermal and moisture properties). In this study, a hydrostatic three-dimensional mesoscale model was used to perform the numerical modeling. The Carlson technique was applied to retrieve the thermal inertia and moisture availability using the thermal AVHRR channels 4 and 5. The net urban effect was determined as the difference between urban and nonurban simulations, in which urban parameters were replaced by rural parameters.

Two winter days were each used for two numerical simulations: a control and an urban-to-rural replacement run. Moisture availability values on the less windy day showed generally a south to north gradient downwind of the city and urban values less than rural values (the urban dry island day). Moisture availability was higher on the windy day, with uniform values in the rural and urban areas (uniform soil moisture day). The only exceptions were variations in the rural hills north of the city and the low rural values under the polluted urban plume downwind of the city.

While thermal inertia values showed no urban–rural differences on the uniform soil moisture day, they exhibited larger values over Atlanta than in surrounding rural area on the (less moist) dry island day. Two puzzling facts exist in the data: 1) lack of a north–south thermal inertia gradient on the dry soil day to correspond to its above-mentioned moisture availability gradient and 2) rural thermal inertia values do not change between both days in spite of their large difference in soil moisture. The observed lack of corresponding urban change is expected, as its thermal inertia values depend more on urban building materials than on moisture of soil.

In both cases both the 2-m and surface skin UHIs showed positive values at night and negative values (an urban cool island, UCI) during the day. The larger nighttime 2-m UHI was on the dry day (0.8° vs 0.6°C), while the larger daytime 2-m UCI was on the moist soil day (-0.3° vs -0.5°C). Note that the surface differences were almost always greater than the 2-m differences.

These day–night differences imply a rural thermal inertia lower than its urban values on both days, which is in conflict with the observations on the wet uniform soil moisture day. On the uniform thermal inertia day (wet day), both the UHI and UCI amplitudes should be less than on the other day, but this is not the case. A possible explanation for both of these conflicts is the improper influence of the urban plume on this day on lowering the thermal inertia and moisture availability values used in the replacement urban simulation.

1. Introduction

Howard (1833a–c) was the first to document the temperature difference between an urban area and its rural environment. This urban–rural temperature contrast was termed the “urban heat island” by Manley (1958) and since then the term has been widely used in the literature.

The urban heat island (UHI), however, is more than a curiosity. According to Changnon (1992), “As of 1991, more than half of all North Americans live and

work in anthropogenically generated urban climates that are drastically different from those in pre-urban (rural) environments of 100 to 150 years ago.” Not only do cities affect the temperature, they affect cloudiness, precipitation, and air quality as well.

Further, the UHI effect is related to the problem of global warming. The majority of weather stations are in cities or nearby; thus, the temperature trend, which is the signature of global warming, can be influenced by urbanization. The effect of urbanization on global temperature trends have been investigated by, for example, Feng and Petzold (1988), Karl et al. (1988), and Karl and Jones (1989), among others. Karl and Jones (1989) found the urban bias in the U.S. climate records (1901–84) to be about 0.06°C for the annual mean and

Corresponding author address: Jan Hafner, CIRA, Colorado State University, Fort Collins, CO 80523-1375.
E-mail: hafner@cira.colostate.edu

0.13°C for the daily minima. This negated the U.S. global warming trend.

The long-term urban bias in temperature data is based on comparison of trends in cities and corresponding rural stations, which may be influenced by urban-rural station configuration, differences in elevation, and local effects. Therefore, to assess and possibly remove the urban bias it is important to understand the net effect of a city.

Numerical models can provide the spatial and temporal variation of UHI and several modeling studies of the UHI have been undertaken. One of the earliest UHI numerical models is by Myrup (1969). In principle, it is a one-dimensional surface energy balance model with parameterized surface energy fluxes (sensible, latent, and soil). The model was applied to a hypothetical city, represented by a concrete slab in the model. He concluded that the main factors leading to UHI development are reduced surface moisture and larger thermal inertia in the city. However, the model did not show the maximum of the UHI at night as indicated by observations.

Johnson et al. (1991) and Oke et al. (1991) developed the Surface Heat Island Model, which is a simple one-dimensional model that predicts surface and subsurface temperatures. It is based on a concept of the force-restore method applied to the soil substrate, and it included radiative contributions from vertical walls. This formulation permitted modeling of the effect of an urban canyon on surface temperatures. The model results under calm clear-sky conditions agreed quite well with observations provided that all input parameters were known with a sufficient degree of accuracy. The main disadvantage was the model's limitation to calm clear-sky conditions and no advection. Later Swaid (1993) modeled the effect of an urban canyon and found a strong effect of the height/width ratio on the street-level temperature and wind flow.

Tapper et al. (1981) investigated the UHI in Christchurch, New Zealand, by using a simple one-dimensional surface energy balance model of Sellers (1969). This model was applied at each grid point over the studied area. Thus, the effect of advection was not considered.

A two-dimensional (vertical plane) urban boundary layer model (URBMET) was developed by Bornstein (1975). It was a hydrostatic, Boussinesq model with two layers: the surface layer (or constant flux layer) and an upper boundary layer, in which the vorticity and heat-conduction equations were applied. Bornstein studied three cases: a rough city, a warm city, and a rough-and-warm city. The main focus was on the effect of an urban area on flow patterns. The warm city's environment was achieved by prescribing surface cooling rates, which were lower in the city than those in the rural neighborhood.

Vukovich et al. (1976) developed the first three-dimensional, primitive-equation numerical model and used it to study the St. Louis UHI. The model's for-

mulation was hydrostatic and adiabatic with prescribed lower boundary conditions including potential temperature. This means that the surface energy balance was not incorporated into the model. St. Louis's UHI was prescribed as an exponentially decaying temperature perturbation from an initial value. The main focus of this study was flow modification by an urban area; again, UHI development was not the objective.

Yoshikado (1992) also used a three-dimensional model to study the urbanized environment and its interaction with the sea breeze in the city of Tokyo. His study was aimed at the response of the sea breeze and urban-induced circulations on the magnitude of the urban heat island. The magnitude of temperature contrast between the city and its surroundings was the input parameter and not the sought variable.

Schayes and Thunis (1990) and later Schayes et al. (1996) improved the URBMET (Bornstein 1975) model to the URBMET/TVM model, which was three-dimensional with topography. This model was used to study urban-topography-induced sea-breeze frontal perturbation over New York City (Bornstein et al. 1993).

Besides these models developed and applied specifically to the study of an urban area, there are other numerical models capable of simulating of an urban-rural complex [an overview of numerical models is given in Thunis and Bornstein (1996)]. Some examples of numerical models used for meteorological phenomena are MM5 (Pennsylvania State University—NCAR mesoscale model) (Dudhia 1993) and RAMS (Regional Atmospheric Modeling System) (Tripoli and Cotton 1982).

A work by Sailor (1995) can be considered as a sensitivity study of the effect of changes in vegetative cover and albedo on the temperature over an urban area. Sailor (1995) used a numerical model to predict the temperature change due to the alternation of albedo and vegetation in Los Angeles. A similar work by Taha (1996, 1997) investigated the impact of albedo and vegetation changes on surface temperature and ozone air quality. The increase in vegetative cover and albedo could be viewed as replacing the urban type of land use/cover by the natural one. However, albedo and vegetation are only two parameters describing a given land use/cover category. Also, the vegetation and albedo were increased by certain values, which may not be related to actual natural conditions prevalent in the Los Angeles Basin.

The three-dimensional modeling approach also accounts for horizontal differences in albedo, surface roughness, and soil properties. A major drawback of all of the above modeling studies is that surface properties, such as, albedo and soil thermal and moisture parameters, were simply assumed. Satellite data incorporation, in the form of the soil parameter retrieval, eliminates their estimation based on a land use/cover categorization. The use of such estimates in urban modeling studies can lead to unrealistically uniform distributions of

the skin surface and 2-m height temperatures within a particular land use/cover category (Hjelmfelt 1982).

Albedo is probably the easiest parameter that can be retrieved from visible satellite data. The soil thermal and moisture properties are more difficult to retrieve. Probably the simplest description of the soil properties is by two parameters: thermal inertia and moisture availability. The thermal channels can be utilized to estimate the thermal properties of soil. The Heat Capacity Mapping Mission (e.g., Price 1979) satellite was designed to monitor the skin surface temperature diurnal range, which is related to the thermal inertia. However, the skin surface temperature is the result of the surface energy balance, which includes sensible, latent, soil, and radiative energy fluxes. This means that soil moisture is an important factor in the skin surface temperature determination, and it is probably the least known parameter in the energy balance.

Microwave systems can be utilized to estimate the soil moisture. For example, Jackson et al. (1992) used a 21-cm passive microwave instrument to retrieve soil moisture over a semiarid area. Active systems, such as SAR (synthetic aperture radar), give better results in soil moisture retrieval, for example, Hirsave et al. (1996). A combination of microwave and optical (visible and/or near-IR remote sensing) can further improve the estimation of soil moisture and surface evaporation. Kustas et al. (1991) attempted to use visible, near-IR, thermal infrared, and microwave data collected from satellite and aircraft platforms to determine various spatially inhomogeneous surface parameters, for example, albedo, soil moisture, and vegetation biomass. Kustas et al. (1993) combined a pushbroom microwave radiometer (21-cm system) and visible and near-IR aircraft data to obtain improved soil and surface evaporation. A similar approach taken by Troufleau et al. (1994) combined *Earth Resources Satellite-1* SAR and Landsat imagery to get improved estimation of sensible and latent heat fluxes. Moran (1990) applied *Landsat-6* TM infrared data in conjunction with Landsat TM red and near-IR data to obtain better spatial resolution for moisture retrieval. Otte and Vidal-Madjar (1994) used satellite remotely sensed IR data to account for vegetative cover and showed their applicability in a hydrological model. The major drawback is the necessity to combine data from several instruments.

Wetzel et al. (1984) proposed a technique to infer soil moisture based on multitemporal satellite data. They used morning IR GOES satellite observations to determine soil moisture. The main advantage is increased temporal resolution, but the horizontal resolution is limited by the GOES IR sensor.

Gillies and Carlson (1995) proposed a new method to infer surface moisture and a vegetation index based on AVHRR thermal and near-IR channels coupled with an inverse modeling scheme and the suggested method compared well with observed data. However, the method does not provide an estimate of the soil thermal

properties, which may limit its applicability in numerical modeling.

The purpose of this work is to improve UHI modeling by use of satellite data to retrieve surface and soil parameters (albedo, soil thermal, and moisture properties) necessary for numerical simulation of UHI characteristic. A method proposed by Carlson et al. (1981) and used in this paper employs satellite data [Advanced Very High Resolution Radiometer (AVHRR)] only to retrieve soil thermal and moisture properties based on two consecutive satellite passes and model simulations.

2. Methodology

a. Model

The Pielke (1974, 1984) model was employed to perform the numerical modeling. This model is a hydrostatic, three-dimensional, primitive-equation model with prognosed horizontal components of wind, moisture, and potential temperature. Vertical velocity and pressure are diagnosed. The model does not include water phase changes, only water vapor is considered. The planetary boundary layer is formulated by a cubic polynomial profile (O'Brien 1970) and by the local gradient Richardson number. O'Brien's profile is employed for unstable boundary layers; a Richardson number formulation is utilized for stably stratified boundary layers. Within the surface layer vertical exchange coefficients are functions of height, wind speed, surface roughness, and mixing length. The surface temperature is determined as a result of the surface energy balance that incorporates net radiation flux, soil heat storage, and sensible and latent heat fluxes. The energy partitioning, and thus the surface temperature, is controlled by these surface characteristics: albedo, surface roughness, soil thermal inertia, and soil moisture.

The model domain was chosen to be 200 km \times 200 km centered near the Atlanta airport with 5-km grid spacing, resulting in a 40 \times 40 grid. The size and spacing of the grid were selected with respect to two constraints. First, the domain should be large enough to minimize the effect of the boundary on the urban area. Second, there is a restriction given by the hydrostatic formulation of the model, which sets the minimum grid spacing to about 5 km. In addition, 5-km grid spacing can reduce navigation errors in satellite data since two consecutive, coregistered skin surface temperature fields are needed for retrieval of soil thermal and moisture properties.

The vertical grid structure was set to increase with height to achieve better vertical resolution near the surface. The vertical levels are as follows: 25, 35, 50, 80, 120, 150, 190, 240, 290, 380, 500, 680, 900, 1200, 1500, 1700, 2200, 2700, 3200, 3700, 4400, 5300, 6500, 7700, and 9100 m above the surface. The wind components and the Exner function are evaluated at these levels, potential temperature and humidity at intermediate lev-

els. The model employs zero gradient lateral boundary conditions.

b. Surface parameters

Four surface parameters are necessary in the Pielke model: albedo, thermal inertia (a combination of required input values of thermal conductivity, soil specific heat, and density), moisture availability, and roughness. The first three parameters can be retrieved from satellite observations. Data from the AVHRR, which flies on the NOAA satellites, were acquired from the Satellite Data Services Division of NESDIS and used in this study.

Albedo can be obtained from AVHRR channel 1 radiometric measurements with calibration information supplied with the data (Kidwell 1995). Unlike the thermal channels (channel 4 and 5), the visible channel is calibrated prior to launch only, and some deterioration of data quality may occur.

Carlson et al. (1981) proposed the following technique to obtain values of the thermal inertia P and the moisture availability M . The thermal inertia is defined by

$$P = \lambda \kappa^{-1/2} = (\lambda \rho_g c_g)^{1/2},$$

where λ is the thermal conductivity, κ is thermal diffusivity, ρ_g is soil bulk density, and c_g is soil specific heat. The moisture availability parameter is given by

$$M = \left(\frac{W}{W_s} \right)^2 \frac{E_{\text{ref}}}{E},$$

where W/W_s is the bulk fractional available moisture content, W_s is the field capacity extractable water content ($W = 0$ at the wilting point), E is evapotranspiration, E_{ref} is reference evapotranspiration corresponding to threshold rate of evaporation at maximum vegetative capillary flow.

A slightly modified approach was applied in this study. The Pielke model was run for 16 different combinations (pairs) of the thermal inertia and the moisture availability, holding other parameters constant. A 21-h simulation was completed for each P - M combination (pair) starting at 0000 UTC. For each P - M combination the modeled skin surface temperature fields were stored at the times corresponding to both satellite observations, about 0900 and 2100 UTC in this case. The observed skin surface temperatures were retrieved by split-window technique (McMillin and Crosby 1984). The split-window technique removes the atmospheric effect of water vapor on satellite-measured brightness temperatures by a linear combination of two IR channels (channels 4 and 5) in the atmospheric window. It should be noted that satellite-derived skin surface temperature refers to the actual surface, which is a mixture of all surfaces within satellite field of view. This may include actual ground, buildings' roofs, top of vegetation, etc.

A bicubic spline was used to describe the two functional relationships between skin surface temperatures

and the two parameters (P and M) at the two times of satellite passage. In other words, at each grid point a combination of P and M is sought (by iteration) such that they will simultaneously match both the daytime and nighttime observed skin surface temperatures.

Surface roughness was estimated rather than retrieved. At each model grid point, the land use/cover was determined from a map supplied by the Regional Resources Development Institute of South Carolina. The surface roughness parameter was assigned to each land use/cover category based on an estimate given in Stull (1988).

c. Assessment of UHI magnitude

The difference between two numerical simulations can be used to estimate the net effect of an urban area as proposed and applied by Hjelmfelt (1982), who studied the city of St. Louis. In the present work, the first numerical simulation (the "urban" simulation) was carried out using retrieved (or estimated) surface input parameters; the second ("nonurban") simulation was accomplished by replacing urban surface parameters by those characteristic of the city's surroundings. The difference between these two numerical runs is defined as the net urban effect or UHI magnitude.

The UHI magnitude is expressed in terms of the temperature at the standard height of 2 m and in terms of the skin surface temperature. The modeled 2-m height temperature can be compared with measurements at weather stations, and the skin surface temperature can be compared with satellite observations. However, the height of 2 m is not a model level. Therefore, the 2-m height temperature is calculated based on similarity from the skin surface temperature and the temperature at the first model level (25 m).

d. Cases selected

Two cases were selected for numerical simulation, namely, 6–7 and 25–26 February 1988, because on these dates clear-sky conditions persisted between two consecutive satellite passes. These are referred to as case 2 and case 1, respectively. The synoptic conditions under which both UHIs developed were similar and almost identical as to the large-scale circulation. In both cases, surface high pressure systems developed over the southeast. The upper-level circulation (at 500 mb) was determined by a low over northern Labrador, resulting in a strong westerly flow over the southeast. The modeled domain was situated on the east side of the surface high with weak surface winds. The wind aloft (500 mb) was characterized by westerly flow with high speeds exceeding 35 m s^{-1} . The surface wind was northwesterly in both cases with speeds about 6 m s^{-1} (6 February) and 2 m s^{-1} (25 February). The topography is given in Fig. 1; Fig. 2 gives locations of weather stations (first order and cooperative).

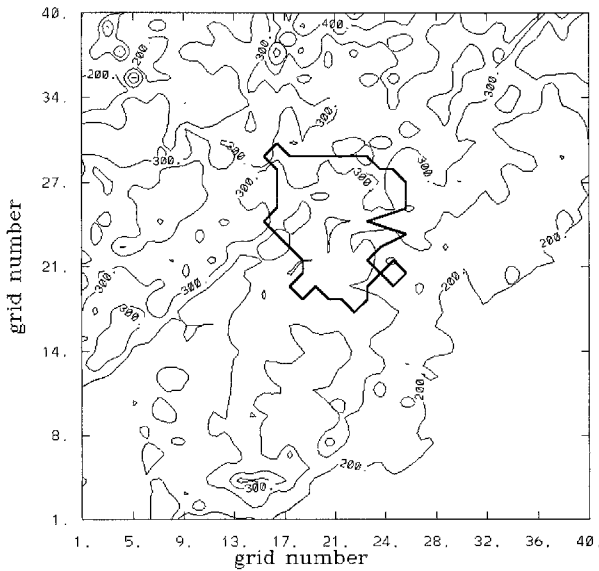


FIG. 1. Topography in the model domain (MSL). The city of Atlanta is outlined.

3. Results

a. Case 1

Three satellite scenes were used for this case, two on 25 February at 0940 UTC (0440 LST) and 2052 UTC (1552 LST), the last on 26 February at 0916 UTC (0416 LST). The last two scenes were cloud free over the Atlanta area. The first scene exhibited slight cloud contamination just southwest of Atlanta; this scene was not used for soil thermal and moisture parameter retrieval. The daytime AVHRR channel 1 data were utilized to obtain the surface albedo, which was assumed to be constant throughout the simulation period.

The final 5 km × 5 km averaged values of albedo are shown in Fig. 3. The urban albedo is about 0.08, which is slightly higher than the albedo of the rural surroundings of about 0.06. It is noticeable that albedo over the whole scene is lower than typical values. The maximum urban albedo is about 0.1. Some typical values of albedos as published in the literature are 0.12–0.14 for industrial complexes and 0.14 for city cores (Sailor 1995). The albedo of an urban area is typically 0.1–0.27 with an average of 0.15 (Pielke 1984, 390–391). Typical values of natural landscapes are within the 0.15 and 0.20 range, for example, a deciduous forest ranges from 0.15 to 0.20 (Pielke 1984), agricultural 0.20, forest 0.18, grassland 0.20 (Sailor 1995). Since albedos of forested areas (~0.20) are higher than an average albedo of an urban area (0.15) more trees in a city will most likely increase the city’s average albedo. Thus, the modeled domain can be considered darker than a typical scene. This can be ascribed to the winter season when vegetation is not fully developed and the brighter, man-made surfaces of the city are more visible.

The retrieved moisture availability parameter is given

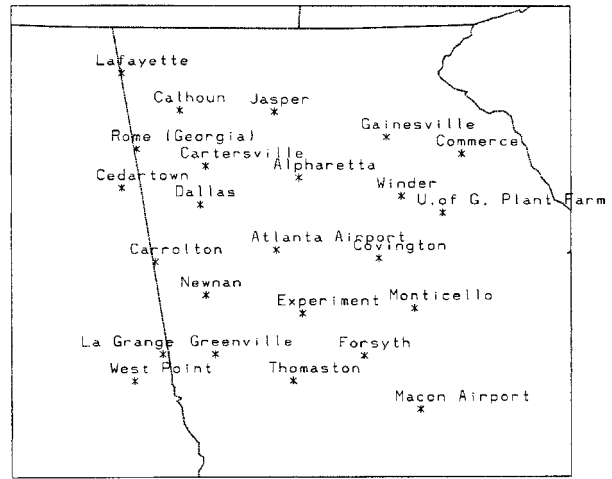


FIG. 2. Weather stations within the model domain.

in Fig. 4, which shows lower urban and higher rural values. The values of the thermal inertia over Atlanta is presented in Fig. 5; it exhibits larger values than the surrounding rural area in contrast to the moisture availability, which shows lower values in the city as compared to the rural area. This may be considered to be typical of an urban–rural complex (Oke 1982). The thermal inertia local maximum of 1.7 kW m⁻² K⁻¹ s^{1/2} just northeast of Atlanta is caused by Lake Sydney Lanier.

The soil moisture and the thermal inertia values are quantities physically related since water changes the bulk specific heat and bulk density of soil. Therefore,

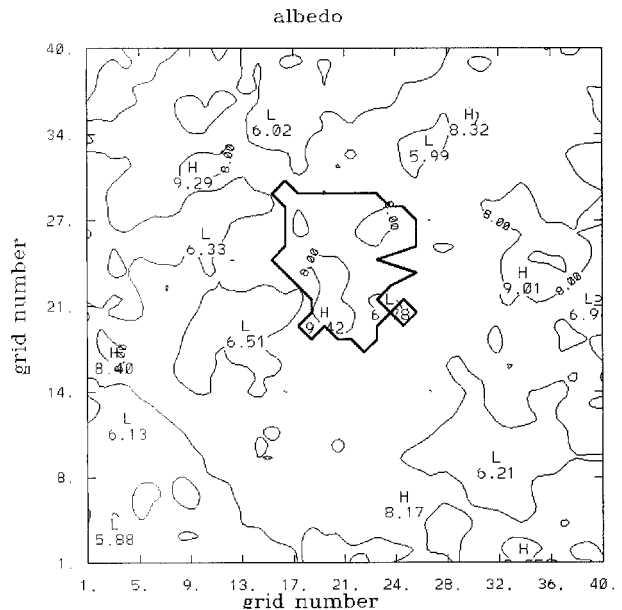


FIG. 3. The 5 km × 5 km averaged values of albedo (%) as retrieved from the channel 1 AVHRR data measured at 2052 UTC (1552 LST) 25 Feb 1988. The thick line outlines the city of Atlanta (the contour interval is 1%).

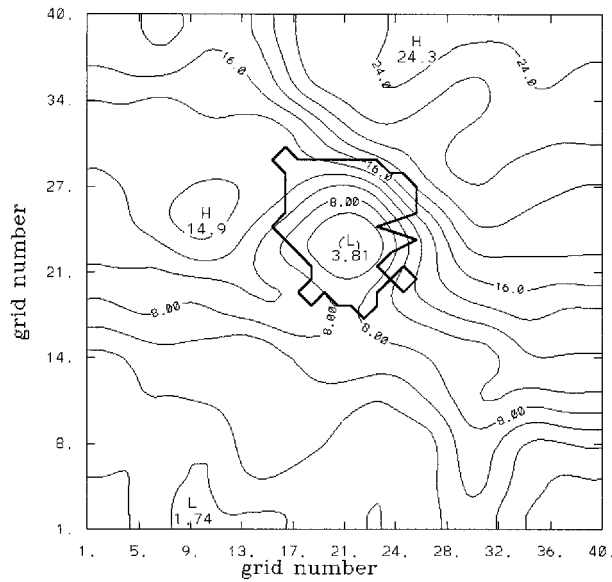


FIG. 4. The moisture availability (%) as determined for 25 Feb 1988. The city of Atlanta is outlined; the contour interval is 2%.

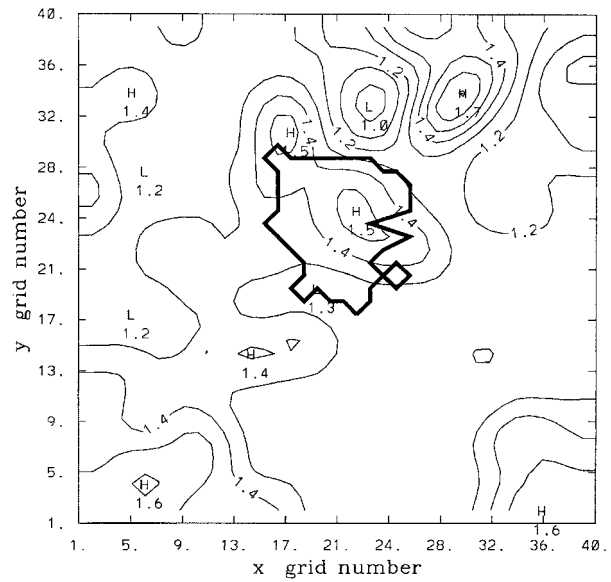


FIG. 5. The thermal inertia ($\text{kW m}^{-2} \text{K}^{-1} \text{s}^{1/2}$) as determined for 25 Feb 1988. The city of Atlanta is outlined (the contour interval is 0.1).

one can expect wet soils have larger thermal inertia than corresponding dry soil. However, this is true only to some extent since moisture availability parameter as defined in this study is rather a measure of evaporation of a particular surface, which includes vegetation. This is a simplified approach that detaches soil moisture and thermal inertia, and thus, a perfect correlation between thermal inertia and moisture availability is not expected. The main reason for application of this approach is that the Pielke (1974) model does not include vegetation explicitly.

The urban–nonurban temperature difference, and thus the modeled UHI magnitude, is expressed in terms of the skin surface temperature and conventional 2-m height temperature. The temporal evolution of the UHI magnitude at one grid point (corresponding to UHI maximum) is shown in Fig. 6. The magnitude of both the skin surface and 2-m height temperature heat islands decreased rapidly from the initial time and by the morning hours the magnitude was near zero. During the day, the magnitude was negative for both the skin surface and 2-m height temperatures with magnitudes of -0.5° and -0.3°C , respectively. In the late afternoon, the UHI recovered its original magnitude of about 0.3° – 0.6°C in the case of 2-m height temperature and about 0.4° – 0.7°C in the case of the skin surface temperature.

The UHI is not uniform spatially. At its maximum near midnight, the UHI magnitude, as indicated by the modeled 2-m height temperature, is about 0.8°C and shows a distinct maximum located in the northeast portion of the city (Fig. 7), near, but not exactly coincident, with the thermal inertia maximum (cf. Fig. 5). There are two areas of negative UHI, a weaker one on the southwest side of the city exhibiting -0.13°C UHI mag-

nitude. The second stronger negative UHI (-0.76°C) is located outside the city’s northern boundary.

The UHI magnitude determined from the skin surface temperature shows slightly different patterns than the 2-m height UHI magnitude. At midnight, near its maximum, the skin surface UHI magnitude (Fig. 8) has a similar 0.8°C maximum but also displays slight negative anomalies, or urban “cool” islands (UCI). During the day the skin surface UCI reached a maximum of -0.7°C .

On average through the simulated period, the UHI magnitude is positive, but it varies substantially and during a significant fraction of daylight hours the city is a UCI. It is noteworthy that daytime skin surface UCI is more negative than corresponding 2-m height UCI magnitude. This is because skin surface temperature

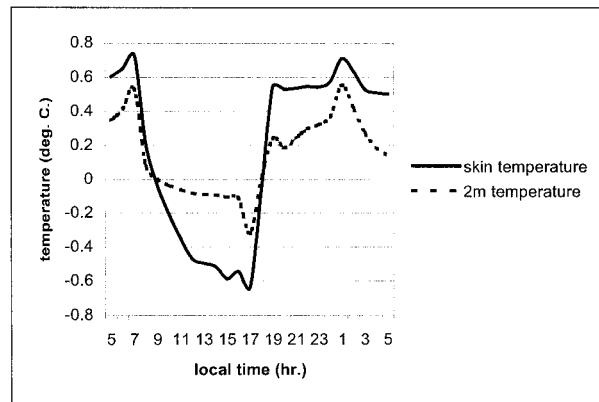


FIG. 6. Temporal evolution of the UHI ($^\circ\text{C}$) at the grid point (22, 27) (a downtown location) in terms of skin surface and 2-m height temperature.

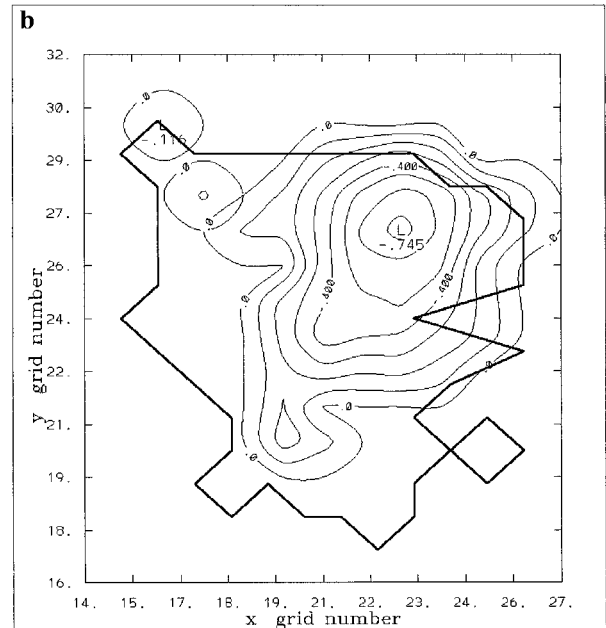
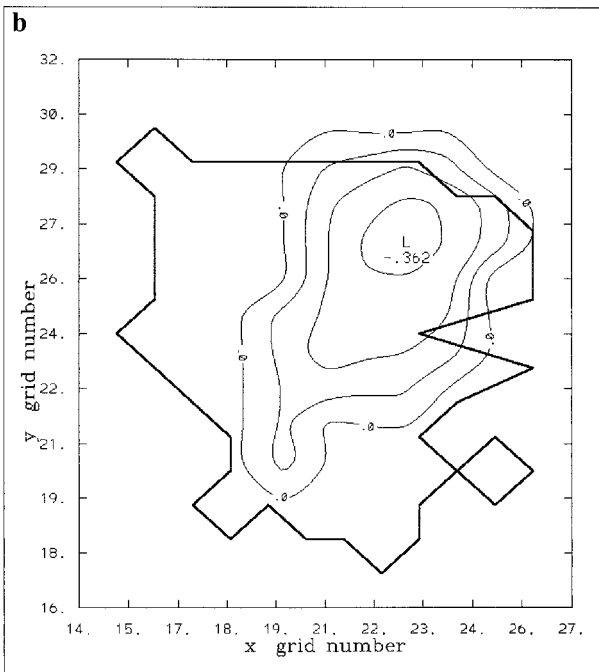
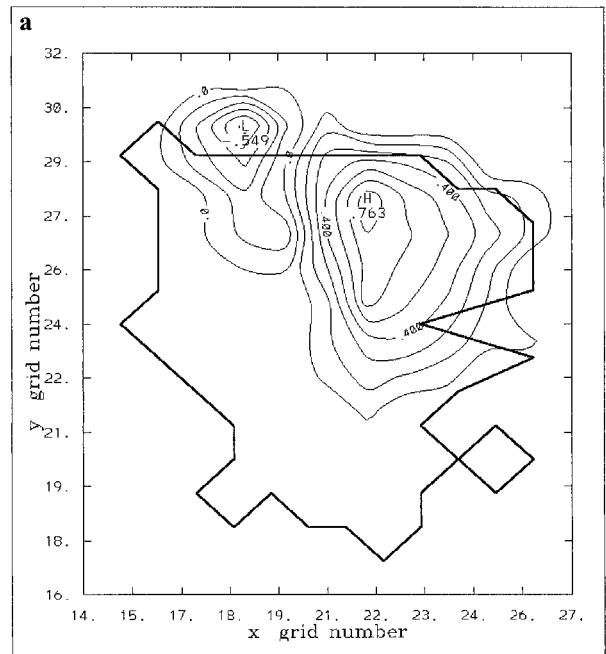
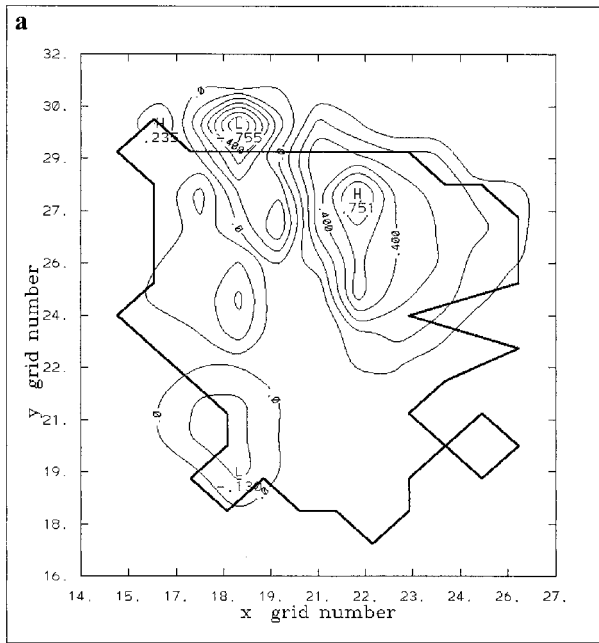


FIG. 7. Horizontal extent of the UHI ($^{\circ}\text{C}$) in terms of 2-m height temperature at (a) 2400 LST 25 Feb 1988 and (b) 1700 LST 25 Feb 1988 (the contour interval is 0.1°C).

FIG. 8. Horizontal extent of the UHI ($^{\circ}\text{C}$) in terms of skin surface temperature at (a) 2400 LST 25 Feb 1988 and (b) 1700 LST 25 Feb 1988 (the contour interval is 0.1°C).

changes more dramatically with changes of albedo, the soil thermal, and moisture properties than 2-m height temperature. The urban effect is simulated by changing values of albedo, surface roughness, and the soil thermal and moisture properties, and, in this case, the nonurban thermal inertia decreased and moisture availability increased. The urban moisture availability is 0.10 and the

corresponding nonurban value is 0.16. The urban thermal inertia is $1.48 \text{ kW m}^{-2} \text{ K}^{-1} \text{ s}^{1/2}$ and the corresponding nonurban value is $1.28 \text{ kW m}^{-2} \text{ K}^{-1} \text{ s}^{1/2}$.

b. Case 2

In this case only two satellite scenes were acquired, the first at 2056 UTC 6 February and the second scene

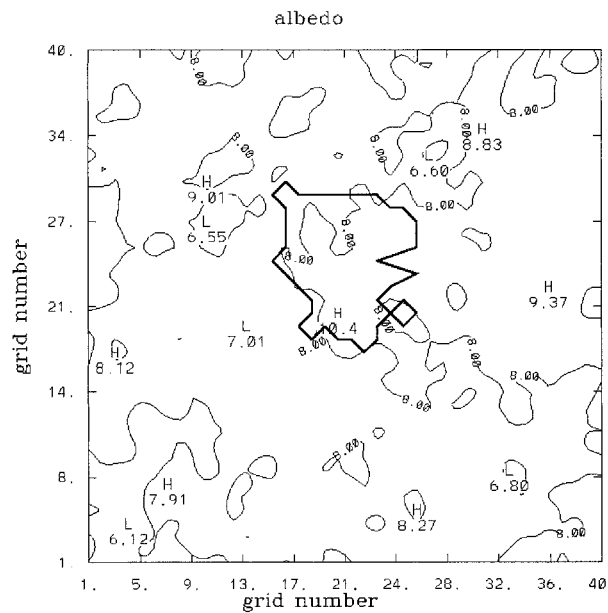


FIG. 9. The 5 km \times 5 km averaged values of albedo (%) as retrieved from the channel 1 AVHRR data measured at 2056 UTC (1556 LST) 6 Feb 1988 (the contour interval is 1%).

at 0921 UTC the next morning. Figure 9 shows 5 km \times 5 km averaged values of albedo. The albedo over the city exhibits higher values than the surrounding area, with a maximum over 0.10 in the southern part of Atlanta. The rural albedos are approximately 0.06–0.09. Both urban and rural albedos in this case were higher than in case 1, in which urban albedo was about 0.08 and rural albedo 0.06. Higher soil moisture as inferred by higher moisture availability would most likely lower the soil albedo. The relationship between albedo and bare soil volumetric water content is inversely proportional (Idso et al. 1975). Experiments performed by Idso et al. (1975) on loam soil showed that albedo increased from 0.14 to 0.32 if volumetric water content decreased from 0.24 to zero. This is opposite to this case in which higher albedos and higher moisture availability were noted. This discrepancy can be ascribed to the effect of vegetation on albedo as presented by Aase and Idso (1975). Aase and Idso (1975) concluded that the albedo–soil moisture relationship is completely destroyed when vegetation is included and that any relationship between remotely sensed albedos and soil moisture content is not possible in a presence of vegetation. Thus, it seems most likely that changes of albedos in this case are due to changes of vegetation.

The thermal inertia and moisture availability were determined as in case 1. The moisture availability field (Fig. 10) shows quite different patterns than in case 1. Here the moisture availability reached extremely high values over 0.6 (compared to about 0.05–0.10 in case 1). Surprisingly, the moisture availability field does not exhibit urban–rural variability as in case 1 but instead a rather uniform distribution. The exceptions are large

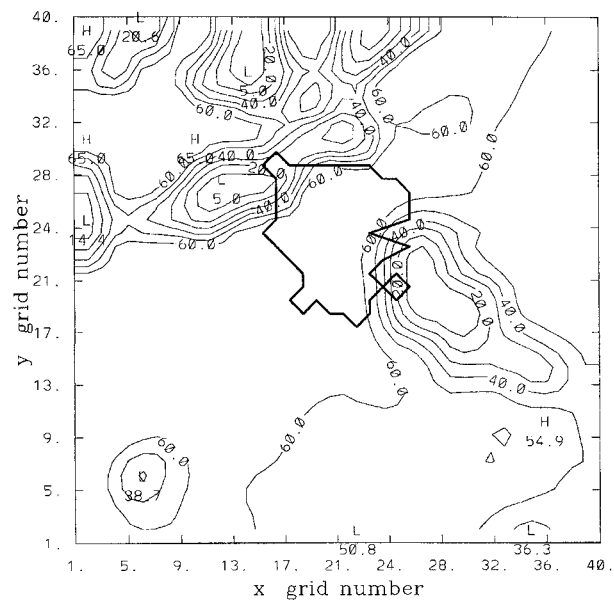


FIG. 10. The moisture availability (%) as determined for 6 Feb 1988. The city of Atlanta is outlined (the contour interval is 10%).

gradient regions northwest of Atlanta and a larger area of lower moisture availability southeast of the city (see Fig. 10). The effect of topography may be the reason for localized minima and maxima northwest of Atlanta. The region of lower moisture availability southeast of the city seems to be the effect of urban plume (Bornstein 1998, personal communication) since this case was associated with northwesterly wind at a speed about 6 m s^{-1} . The absence of the effect of an urban plume in case 1 may be due to calm conditions on that day (northwesterly wind at ~ 2 m s^{-1}).

Figure 11 shows the thermal inertia field over the modeled domain. The patterns are similar to the moisture availability exhibiting local maxima and minima in a hilly region northwest of Atlanta, maximum at Lake Sydney Lanier, and a larger area of lower thermal inertia southeast of the city. The low values of the thermal inertia southeast of Atlanta can be the effect of an urban plume. The urban values of the thermal inertia do not vary significantly across the model domain with the above-mentioned exceptions. There is a small variation of the thermal inertia within a city that shows a maximum at the city's center (see Fig. 11, within the 1.20 contour) and lower values on the city's boundary.

The possible effect of urban plume on the soil thermal and moisture retrieval can be estimated in case 2 since the rural thermal inertia and moisture availability show little variation and can be used as background reference values (Fig. 10 and Fig. 11). The urban plume lowers both the thermal inertia and moisture availability as retrieved from satellite data. This means that the effect of urban plume on satellite-retrieved temperatures will be an increase of the diurnal range of the skin surface temperature (higher daytime and lower nighttime skin sur-

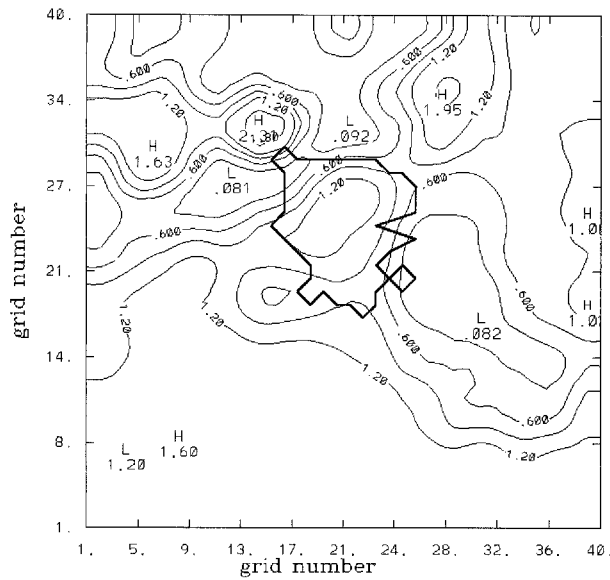


FIG. 11. The thermal inertia ($\text{kW m}^{-2} \text{K}^{-1} \text{s}^{1/2}$) as determined for 6 Feb 1988. The city of Atlanta is outlined (the contour interval is 0.3).

face temperatures). If the polluted urban plume decreases the retrieved thermal inertia and moisture availability, then the correct urban values of these parameters should be higher in case 1, in which the plume resided over the city due to calm wind conditions. Since the urban maximum of the thermal inertia in case 1 is already higher than the corresponding value in case 2, then removing the effect of the urban plume will increase its value even more. This seems to be in conflict with the fact that urban thermal inertia usually does not change very much with changes of soil moisture, as it depends more on building materials than on soil moisture. The possible explanation can be the different effects of the urban plume on skin surface retrieval in both cases as they differ in wind conditions. Then one can expect an urban dome rather than an urban plume under calm conditions of case 1. In this case the polluted urban plume (dome) would be deeper and probably more polluted than on a windy day (case 2). A more detailed investigation will be needed to establish an accurate assessment of the effect of urban plume on satellite-based skin surface temperature retrieval and, thus, on thermal inertia and moisture availability.

Comparing rural values of the thermal inertia on both days shows almost no change of its magnitude with the exception of the area under the urban plume on a windy day (case 2). This fact that the rural thermal inertia has not changed is somewhat puzzling since it should reflect to some extent a dramatic increase of the moisture availability in case 2. It may be due to interception of rainfall water on a surface (ground or vegetation) rather than infiltration into soil. In this case the moisture availability will increase, whereas the soil thermal inertia will not

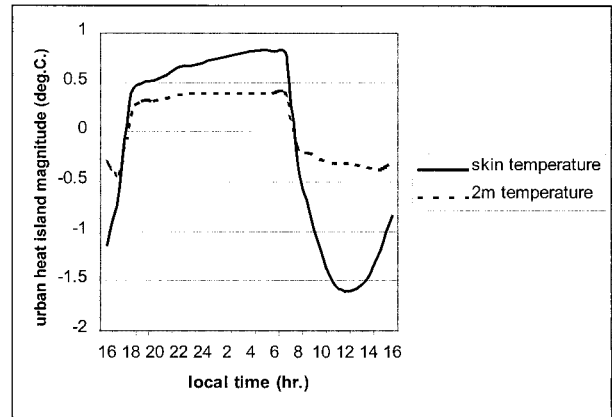


FIG. 12. Temporal evolution of the UHI ($^{\circ}\text{C}$) at the grid point (22, 27) (downtown) in terms of skin surface and 2-m height temperature on 6 and 7 Feb 1988.

change significantly. However, resolving this conflicting fact will require further study.

After the completion of the urban and nonurban simulations, the UHI magnitude was calculated. The temporal evolution of the UHI at grid point (22, 27) is shown in Fig. 12. The daytime UHI exhibits negative values in contrast to the positive nighttime magnitudes. This pattern is similar for both skin surface and 2-m height UHIs, only the magnitude is smaller in the case of 2-m height temperatures. Also this is consistent with the results of case 1 as to the temporal and spatial evolution of UHI.

The spatial distribution of UHI in terms of skin surface and 2-m height temperature is given in Figs. 13 and 14. The maximum positive UHI was determined to be 1.2°C for skin surface temperatures (0.6°C for 2-m height temperatures). The negative daytime UHI was -2.1°C for skin surface temperature and about -0.5°C for the 2-m height temperature. The larger magnitude of UCI implies larger values of the urban thermal inertia than rural values and, since moisture availability is almost uniform, the UCI is mostly the effect of the thermal inertia. This seems to be in conflict with the retrieved field of the thermal inertia, which does not show expected contrast between urban and rural values across most of modeled domain (except the hilly area northwest of Atlanta and the area under the urban plume, see Fig. 11). The possible reasons for the lower nonurban values of the thermal inertia in nonurban replacement simulation may be the effect of the area of low values under polluted urban plume southeast of the city.

4. Verification of model results

Satellite-derived skin surface temperatures and in situ data from cooperative stations located within the modeled domain and from one first-order weather station at the Atlanta airport are available for model verification (see Fig. 2).

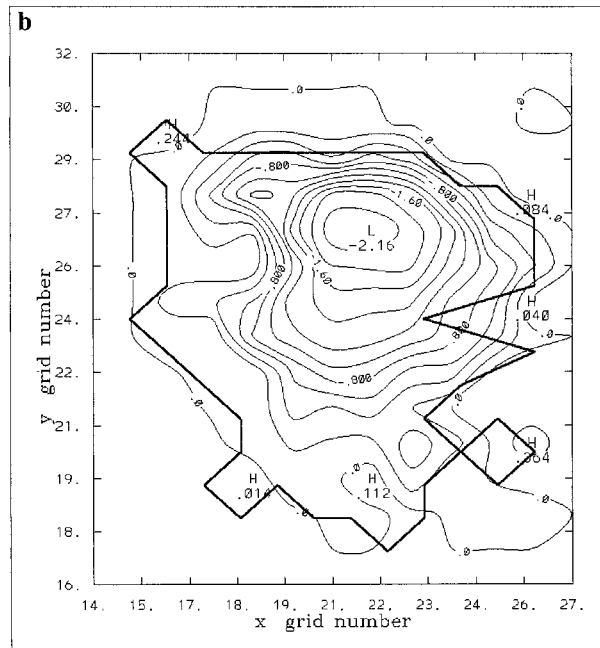
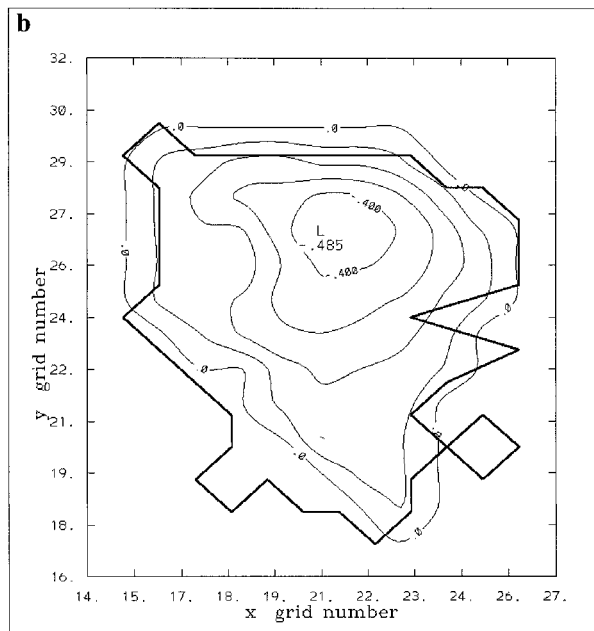
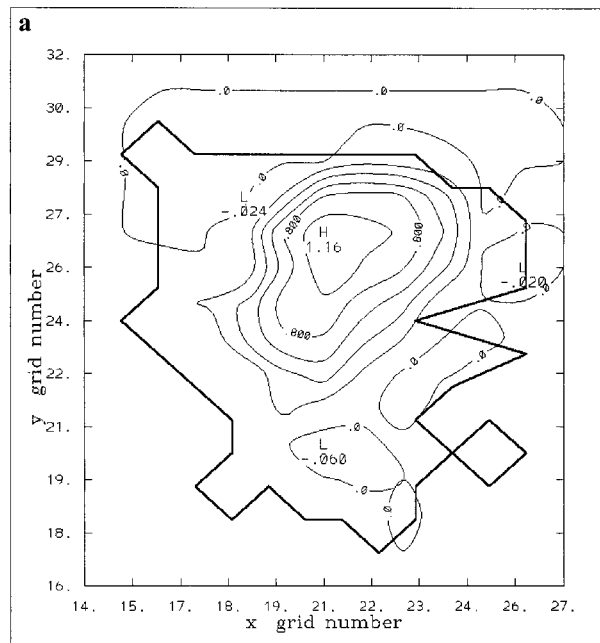
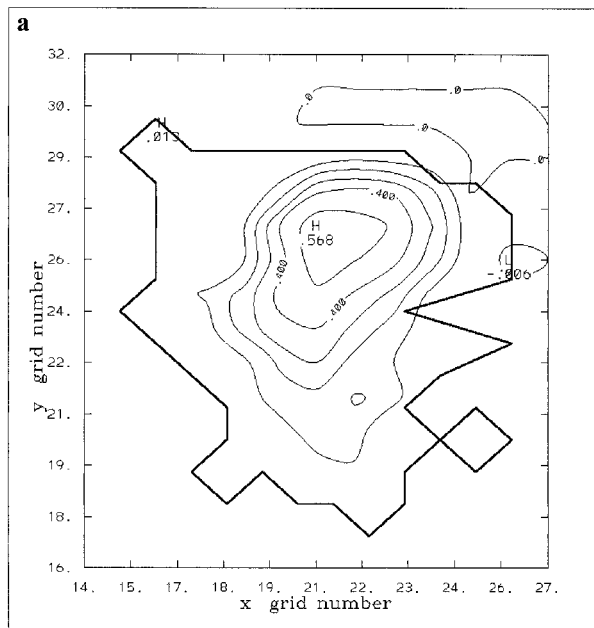


FIG. 13. Horizontal extent of the UHI ($^{\circ}\text{C}$) in terms of 2-m height temperature at (a) 0600 LST 7 Feb 1988 and (b) 1200 LST 7 Feb 1988 (the contour interval is 0.1°C).

FIG. 14. Horizontal extent of the UHI ($^{\circ}\text{C}$) in terms of skin surface temperature at (a) 0600 LST 7 Feb 1988 and (b) 1200 LST 7 Feb 1988 (the contour interval is 0.2°C).

a. Case 1

A comparison of hourly measurements of temperature at the Atlanta airport [model grid (20, 22)] and corresponding modeled 2-m temperatures on 25 and 26 February is given in Fig. 15. The difference of modeled and measured temperatures is within 2°C , but there is a phase difference. The modeled 2-m height temperature leads the observed temperature by about 2 h.

The differences between satellite-observed and modeled skin surface temperature at two times are shown in Fig. 16. Since the soil thermal and moisture properties were selected such that the model would reproduce observed skin surface temperatures, near-zero difference is expected, but there were differences. The largest difference was about -6.3°C in the early morning (0416 UTC, Fig. 16b) located on the northern (inflow) bound-

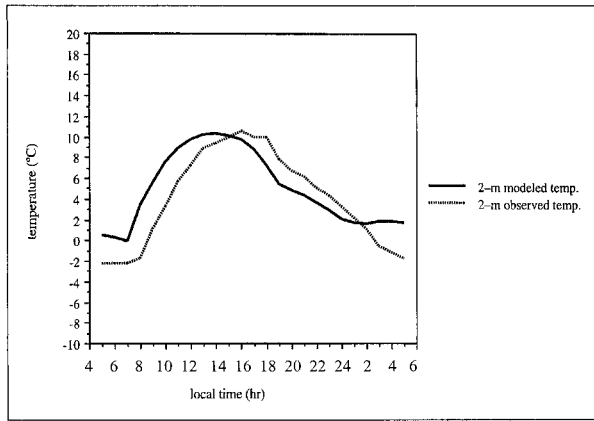


FIG. 15. Time plot of modeled and observed 2-m height temperatures (°C) at the Atlanta airport [model grid (20, 22)] on 25 and 26 Feb 1988.

ary, which may be the effect of the boundary or, more probably, the local effect of topography. The overall error in the urban area is about 0°–1°C on 25 February at 2052 UTC (1552 LST), which means that the model simulated cooler temperatures than observed. At 0916 UTC (0416 LST) 26 February, the errors were negative, with about a –2°C departure in the urban area, which corresponds to warmer modeled temperatures than observed.

The maximum temperatures measured at the cooperative stations are compared to the modeled maxima at the corresponding grid points in Fig. 17a. The overall difference is positive and exhibits a maximum of 5°C at Forsyth (located southeast of Atlanta), which seems to be extremely large and not representative of the whole domain. The overall temperature departure is about –1° to 1°C over the urban area. Figure 17b gives the spatial distribution of the minimum temperature errors, which are negative. The largest error of –7°C is located at Greenville, south of Atlanta. Across the urban area, the temperature errors are within the range –2°–4°C. The larger departures for the temperature minima than for the maxima may be a local effect, for example, accumulation of a cool air in a valley.

b. Case 2

The comparison of the modeled and observed 2-m height temperatures at the Atlanta airport is presented in Fig. 18. The pattern of the diurnal cycle is clearly expressed; the agreement of modeled values and the observation is within a reasonable limit (about 2°C). The model tends to predict warmer temperatures at night and morning, cooler in afternoon. The maximum departure of modeled and observed temperature occurred during the early morning (~4°C), at night the error was about 2°–3°C. It should be noted that the measurements on 7 February at 1300, 1400, 1500, and 1600 LST were

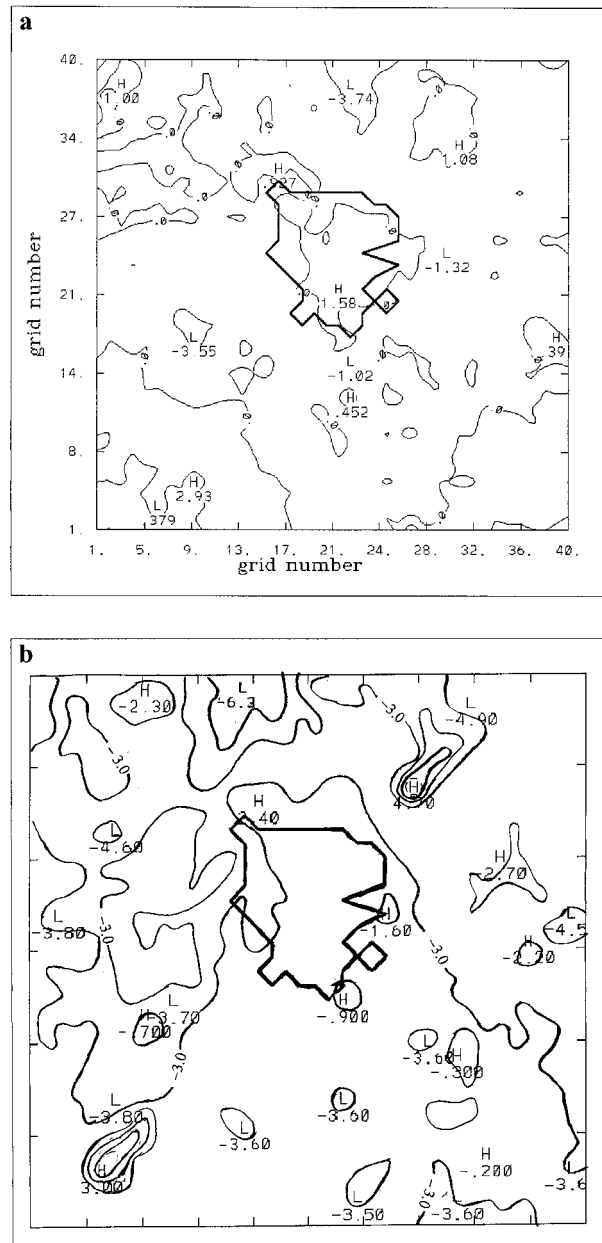


FIG. 16. The difference between satellite-observed and modeled skin surface temperatures (°C) at (a) 2052 UTC 25 Feb 1988 and (b) 0916 UTC 26 Feb 1988 (the contour interval is 2°C).

affected by clouds covering 1/10 at 1300 LST and 10/10 thereafter.

Because only two satellite-observed skin surface temperature fields were available, the comparison of the modeled and observed skin surface temperatures was performed for the only second scene—0921 UTC (0421 LST) 7 February 1988. The satellite-derived skin surface temperatures at 2056 UTC (1556 LST) 6 February are identical to the modeled ones since they were used for model initialization. The resulting difference between the satellite-retrieved and modeled skin surface

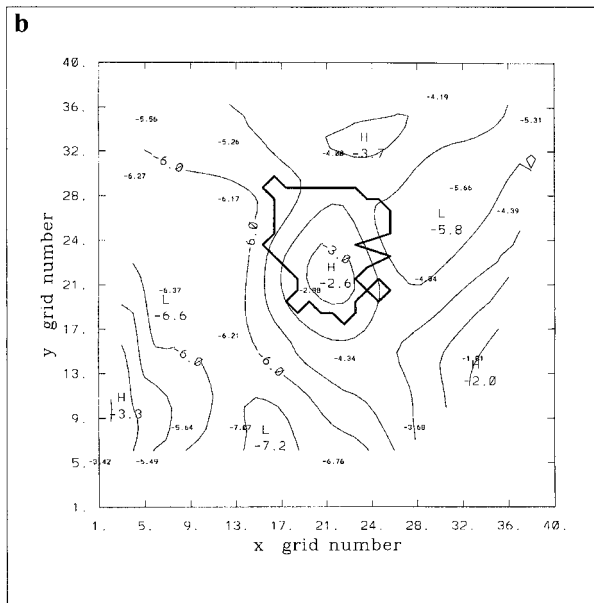
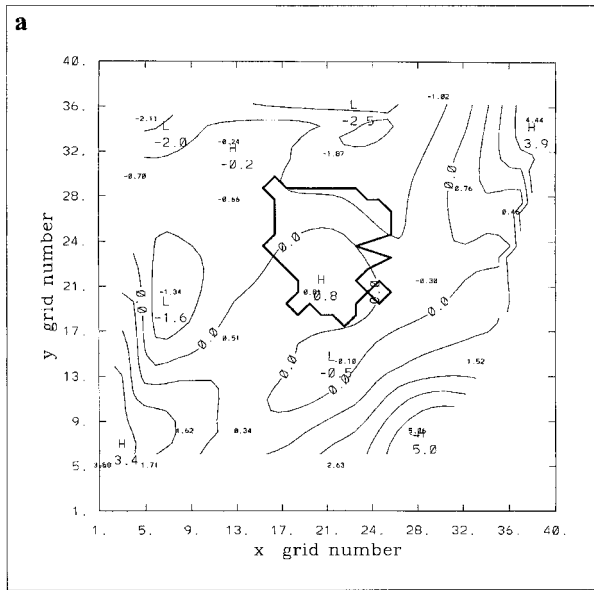


FIG. 17. The difference of the 2-m height (a) maximum temperatures ($^{\circ}\text{C}$) observed at the cooperative stations and the corresponding modeled maxima on 25 Feb 1988 and (b) observed minimum temperatures at cooperative stations and corresponding modeled minima on 26 Feb 1988 (the contour interval is 1°C).

temperatures are in Fig. 19. The largest error in the skin surface temperatures is 8.2°C located northeast of Atlanta near Lake Sydney Lanier; it is most probably the effect of the lake. The typical error over the city is about -1.0° to $+1.0^{\circ}\text{C}$.

The difference between modeled and observed temperature minima is shown in Fig. 20a. The difference is negative in this case, which implies that the model simulates warmer temperatures than observed at the cooperative stations. The difference exhibits a magnitude

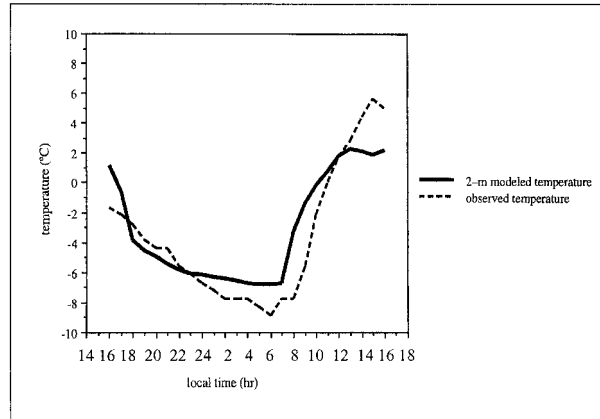


FIG. 18. Time plot of modeled and observed 2-m height temperatures at the Atlanta airport on 6 and 7 Feb 1988. Note that the measurements at 1300, 1400, 1500, and 1600 LST 7 Feb were affected by clouds.

of about -4.0° to 1.0°C over the urban area. The maximum departure of -7.8°C of the modeled and observed value of the minimum temperature is located northwest of Atlanta at the Dallas station.

The difference for the maxima shows negative as well positive values, as plotted in Fig. 20b. The regions exhibiting negative differences are located on the northwest and southeast corners of the domain. The positive departures are found on the northeast and southwest sides of the model domain. This means that the model overestimates the maxima in regions northwest and southeast of Atlanta and underestimates them elsewhere. The overall departure in the city is about -5.0° – $+1.0^{\circ}\text{C}$.

Based on the previous comparison of the simulated

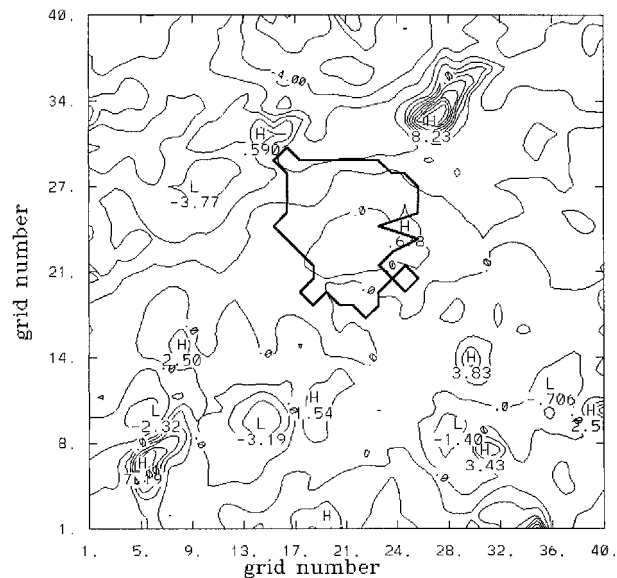


FIG. 19. The difference ($^{\circ}\text{C}$) between satellite-observed and modeled skin surface temperatures at 0921 UTC (0421 LST) 7 Feb 1988 (the contour interval is 1°C).

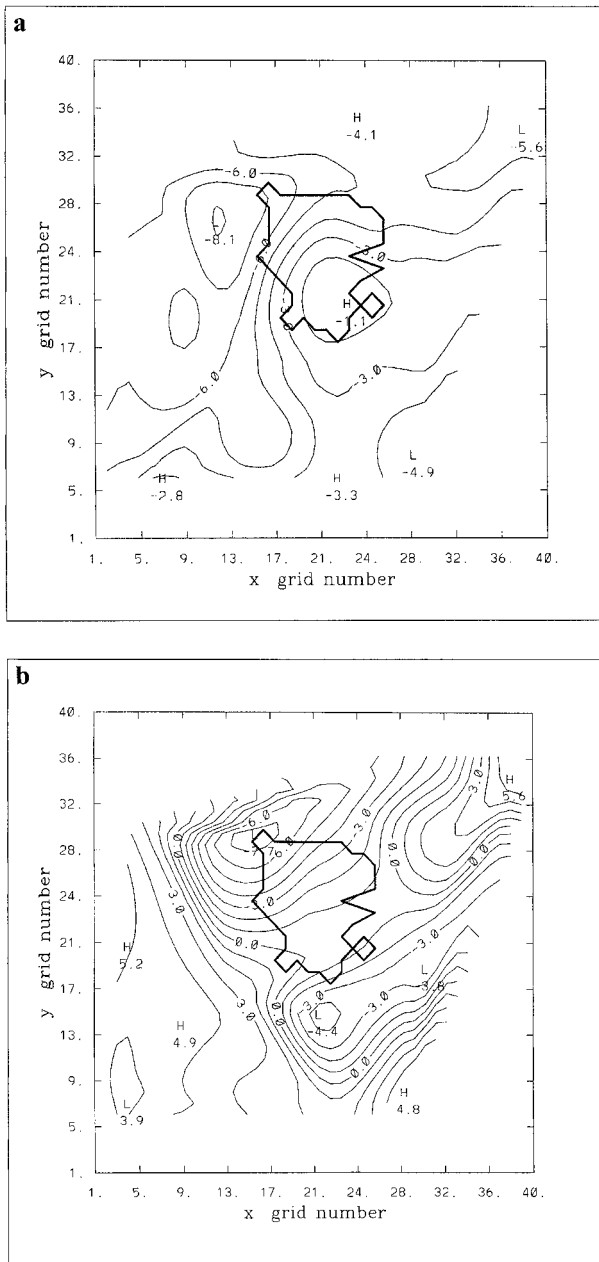


FIG. 20. The difference ($^{\circ}\text{C}$) of the 2-m height (a) minimum temperatures observed at the cooperative stations and the corresponding modeled minima on 7 Feb 1988 and (b) maxima observed at cooperative stations and the corresponding modeled maxima on 7 Feb 1988 (the contour interval is 1°C).

skin surface and 2-m height temperatures with corresponding observations, the model tends to predict cooler temperatures during late afternoon and at night than observed. Early and late morning modeled temperatures are warmer than observations.

The fact that the comparison of the modeled and observed skin surface temperatures did not yield zero difference can be attributed to the different model setup

used for soil parameter retrieval. A reduced 10×10 grid was used instead of the 40×40 grid of the actual simulations. In addition, the retrieval technique assumes horizontal homogeneity of thermal inertia and moisture availability, which is not the case of the actual model runs. The large errors in both cases for modeled and observed temperature extremes (maxima and minima) seem to be due to surface parameterization. Observations were taken at cooperative stations that are located at one spot and may not always be representative for a larger area, for example, $5 \text{ km} \times 5 \text{ km}$ in this case. Also the model tends to average temperature extremes over a grid box. Local features that are spatially smaller than a grid size are not captured in the model and cannot be resolved, for example, a small valley in which cold air can accumulate. Also, the model is incapable of resolving the internal structure of the so-called urban canopy. Thus, the modeled skin surface temperature will be different from that at street level.

5. Energy balances

The UHI magnitude based on either skin surface or 2-m height temperature is determined mainly by the surface energy balance. The energy balance components are evaluated at model ground level, more precisely at z_0 (roughness length) level above the ground. In a presence of denser and higher vegetation this level may be a displacement height above the actual ground level, and then the model surface corresponds to the top of vegetation (or built-up area). However, the model does not take into account the displacement height and assumes that the top of vegetation is the model's ground level. This means that the model is not capable of determining air temperature within a vegetation canopy or at street level in an urban canyon.

Therefore, to determine the main cause of the UHI development it is necessary to investigate the difference in the surface energy balance between the urban and nonurban cases. The surface energy balance components were determined by the numerical simulations, and the following discussion is based on model results.

a. Case 1

The energy partitioning at a grid point (22, 27) is given in Fig. 21. The selection of the point (22, 27) was determined by the fact that it is close to the local UHI maxima in both studied cases. Positive values represent energy gain; negative, energy loss. Incoming solar radiation is expressed in terms of energy absorbed, that is, the effect of the albedo is included. During the day the sensible, latent, and soil heat fluxes are sinks of incoming energy; at night they represent energy sources. Among these three components, the soil heat flux is the most significant, reaching its largest magnitude near noon. The latent heat flux is negligible compared to the other energy balance components. This may be the result

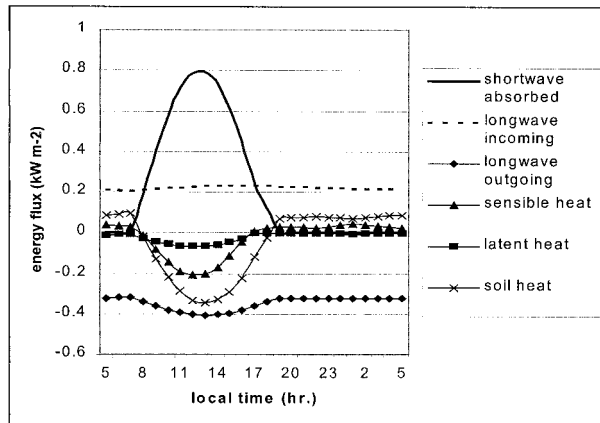


FIG. 21. The surface energy components (kW m^{-2}) at a downtown grid point (22, 27) on 25 and 26 Feb 1988.

of dry conditions found in the urban area as indicated by the very low value (less than 0.10) of the moisture availability. The magnitude of the moisture availability parameter determined for Atlanta's surroundings is about 0.10–0.15, that is, more than 50% of the urban value. However, even these values represent relatively dry surface conditions.

To examine the main factors controlling the UHI development, the difference of the surface energy balance components between the urban and nonurban simulations was determined (Fig. 22). The magnitude of the energy flux difference is on the order of several watts per square meter. The difference of the shortwave absorbed energy is negative, which means that the urban location absorbs less solar energy than a corresponding nonurban location. This is simply the result of the decreased albedo for the nonurban simulation. The urban value of the albedo at grid point (22, 27) is 8.0%; the corresponding nonurban value is 7.4%. In this respect, this is not a typical situation. Usually an urban area exhibits lower values of albedo than rural areas. Therefore, in this particular situation, the absorbed solar radiation would lead to an urban cool island due to the higher urban albedo.

The incoming longwave radiative flux is almost identical for both urban and nonurban simulations. Thus, this term does not contribute to temperature differences. The difference of the sensible heat flux is positive during the day and slightly negative at night.

The difference in the latent heat flux exhibits positive values that peak early in the afternoon, which is the result of the lower moisture availability in the urban area. The urban value of the moisture availability at grid point (22, 27) is 0.10, compared to the corresponding nonurban value of 0.16. Positive values of the energy flux difference would contribute to the UHI. In addition, in this situation the magnitude of the latent heat difference is the second largest ($\sim 45.7 \text{ W m}^{-2}$), comparable only to the absolute value of the soil heat flux difference.

The difference in the soil heat fluxes exhibits the

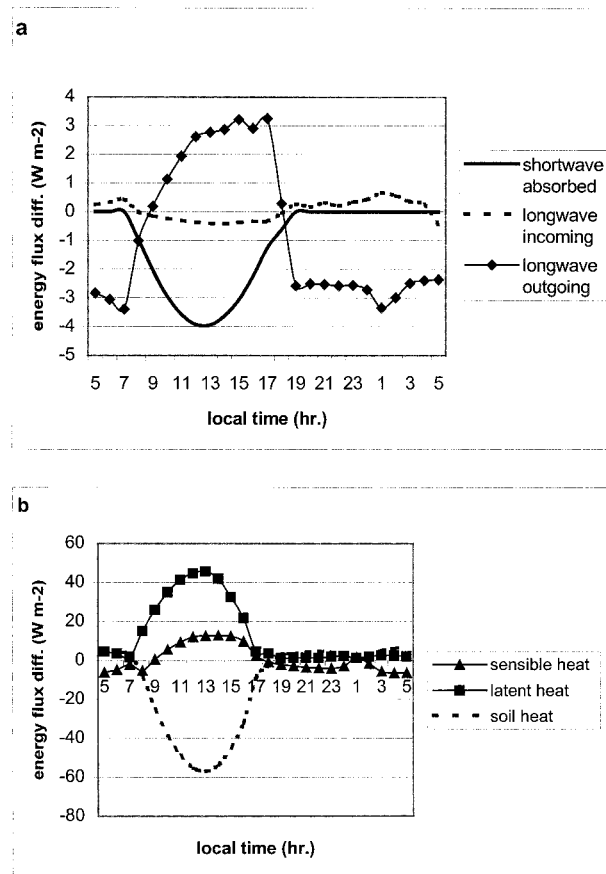


FIG. 22. The difference of the surface energy balance components (W m^{-2}) between the urban and nonurban simulations at a downtown grid point (22, 27) on 25 and 26 Feb 1988 for (a) shortwave absorbed, longwave incoming, and longwave outgoing flux components; and (b) for sensible heat, latent heat, and soil heat components.

largest absolute value (-56.9 W m^{-2}) also near noon. This is the result of the lower thermal inertia of the nonurban replacement case. The urban value of the thermal inertia is $1.48 \text{ kW m}^{-2} \text{ K}^{-1} \text{ s}^{1/2}$, compared to the corresponding nonurban value of $1.28 \text{ kW m}^{-2} \text{ K}^{-1} \text{ s}^{1/2}$. In this case, during the day, the soil heat flux difference is negative; during the night it shows positive values. This means that during the day the difference in the soil heat flux contributes to the UCI. At night the situation is reversed, that is, positive values of the soil heat flux difference contribute to the positive UHI. Generally, a larger thermal inertia results in a larger heat sink during the day and larger heat source during the night, which corresponds to this situation.

Based on the above discussion, the daytime and nighttime situations are different in their energy partitioning. During the day, the latent, soil, and sensible energy fluxes are the major components in UHI development. At night the situation is different; there are only two major components: the positive soil heat flux difference and compensating negative sensible heat flux difference.

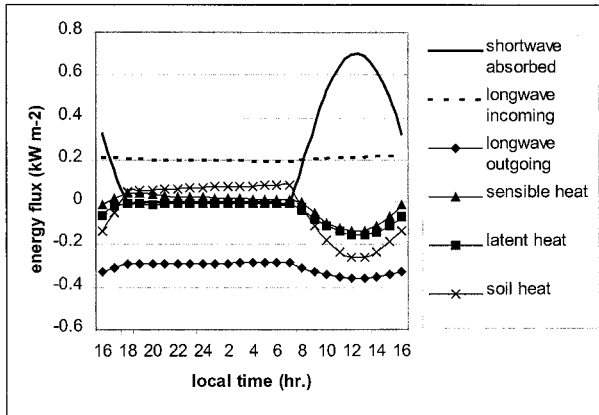


FIG. 23. The surface energy components (kW m^{-2}) at a downtown grid point (22, 27) on 6 and 7 Feb 1988.

b. Case 2

Figure 23 shows the components of the surface energy balance as determined at grid point (22, 27). At night the soil heat fluxes is positive, representing source terms. In turn, the daytime soil, sensible, and latent heat fluxes exhibit negative values, which correspond to a sink of energy. Latent and sensible heat fluxes are almost zero (or negligible) at night. There is one difference between the energy partitioning in case 1 and case 2: daytime latent heat flux. In case 2 the latent heat flux reached a larger magnitude than that in case 1. This is certainly the result of the extremely high values of the moisture availability in case 2. The moisture availability at grid point (22, 27) is 0.65, compared to the case 1 value of only 0.10.

Figure 24 shows the difference of the surface energy balance components between the urban and nonurban case at the downtown grid point (22, 27). The difference of the radiative components, that is, incoming longwave and absorbed shortwave radiation, is much less compared to other components. This means that radiative components do not contribute to the UHI development. The urban albedo is 7.8% and the corresponding nonurban value is 8.0% at grid point (22, 27). This small difference of the albedo results in about 1.4 W m^{-2} difference of the incoming absorbed shortwave radiation.

The difference of the other components, namely, soil, latent, and sensible heat, contributes to the UHI. As the difference of the outgoing longwave radiation is the result of the urban heat itself, and it does not contribute to the UHI development. In this case the most significant component of the surface balance is the soil heat flux, which exhibits the largest magnitude of urban–nonurban difference. Two distinct regimes can be distinguished: the first one at night, the other during the day. At night the difference of the soil heat flux is positive, unlike the sensible heat, which shows the negative differences. The latent heat difference is close to zero and, thus,

does not contribute significantly to the UHI. Since the magnitude of the soil heat flux difference is larger than that of the sensible heat, it results in a positive UHI. During the day the situation reverses; the soil heat flux difference exhibits a larger magnitude than the sensible and latent heat differences, and the result is a negative UCI.

Therefore, it can be concluded that the main reason for the UHI is the soil heat flux difference, which is caused by the lower value of the thermal inertia for the nonurban case. The urban value of the thermal inertia at this particular grid point is $1.32 \text{ kW m}^{-2} \text{ K}^{-1} \text{ s}^{1/2}$ and the corresponding nonurban value is $0.63 \text{ kW m}^{-2} \text{ K}^{-1} \text{ s}^{1/2}$.

6. Conclusions

The UHI development was modeled for two different cases, 25–26 and 6–7 February 1988. The moisture availability in case 1 exhibits lower values, 0.04, within the city as compared to rural values of about 0.1 (see Fig. 4). The maximum of 0.24 over the whole domain is located to the north of Atlanta. Case 2 is characterized by extremely large values of moisture availability, reaching a maximum about 0.65 (see Fig. 10). The city does not show lower values, but it exhibits almost uniform distribution. The differences between the moisture availability spatial distribution between case 1 and case 2 may be due to the preceding rainfall. The 14-day cumulative rainfall in case 1 ranges from 3.8 to 30.3 mm, whereas in case 2 40–160-mm cumulative rain amounts were observed.

The thermal inertia in case 2 shows a better correlation with the moisture availability (correlation coefficient 0.67) than in case 1 (correlation coefficient -0.44). This poor correlation in case 1 can be seen in Figs. 4 and 5 where there is a south to north gradient in the field of the moisture availability that is completely missing in the thermal inertia field. In both cases Lake Sydney Lanier appears as a local maximum in the thermal inertia field. It is noteworthy that the thermal inertia has not changed significantly from case 1 to case 2, whereas the moisture availability shows a substantial increase in case 2. The lack of a south to north gradient of the thermal inertia in case 1 and almost no change of its magnitude in case 2 are two unexplained facts. Resolving this conflict will require more research.

The effect of a polluted urban plume on the moisture availability and thermal inertia is seen in case 2 as an area of lower values downwind of the city (Figs. 10 and 11). Case 1 does not show this effect so clearly due to calm wind conditions (wind speed about 2 m s^{-1}) in which the plume resided over the city. Nevertheless, the effect of the urban plume in this case can be detected based on observed and modeled 2-m height temperatures at the Atlanta airport (Fig. 15), indicating lower thermal inertia in the model, which is exactly the effect of the urban plume.

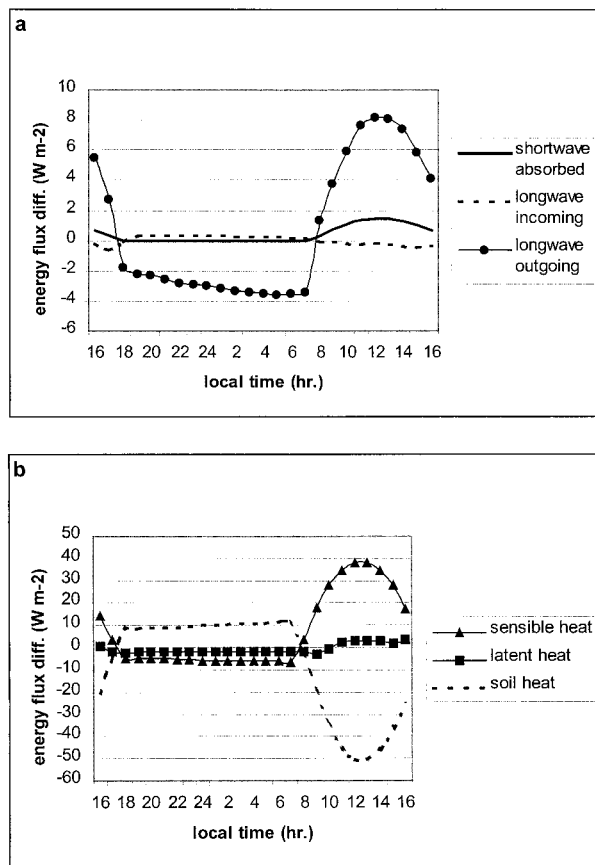


FIG. 24. The difference of the surface energy balance components (kW m^{-2}) between the urban and nonurban simulations at a downtown grid point (20, 24) on 6 and 7 Feb 1988 for (a) shortwave absorbed, longwave incoming, and longwave outgoing components; and (b) sensible heat, latent heat, and soil heat components.

The difference in the surface energy fluxes between the urban and nonurban simulations is the key factor in UHI development. As seen in Fig. 22, the daytime development of the UCI in case 1 is the result of latent, sensible, and soil heat flux differences. The latent heat flux difference contributes only to the daytime UCI, at night its magnitude was negligible. The nighttime maximum was about 0.8°C for both skin surface and 2-m UHI and daytime UCI exhibited -0.3°C at the 2-m height and -0.7°C for the skin surface UCI.

Case 2 shows that the daytime UHI is the result of the soil and sensible heat flux differences, that is, unlike the first case, latent heat flux difference is not important even during the day (see Fig. 24). The resulting maximum was 0.6°C for 2-m height and $+1.2^{\circ}\text{C}$ for skin surface UHI; the daytime UCI magnitudes were -0.5°C and -2.1°C for 2-m height and skin surface UCI, respectively.

In both cases the UHI was simulated in the terms of the skin surface and 2-m height temperatures, and significant variability of the UHI was found in the spatial and temporal evolution. It can be seen almost as a gen-

eral pattern that the skin surface-based UHI exhibited larger magnitudes (positive or negative) than the 2-m height temperature UHI. This is because the surface experiences a larger diurnal variation of temperature than at the 2-m level as a result of upward energy transfer from the surface. In both cases the UHI is manifested as a nocturnal phenomenon; during the day the UHI actually reverses into a UCI. The difference of the urban and corresponding nonurban albedos seems to be less important than other factors, at least in the winter season.

In conclusion, the main factors contributing to the UHI development in the model were identified in both cases. The difference between the nighttime and daytime UHI can be distinguished. The principal components responsible for the UHI development are soil and sensible heat fluxes at night. During the day all three surface-related fluxes, namely, soil, sensible, and latent heat flux, can be important depending on the situation. In relatively dry urban conditions, the latent heat flux difference is significant during the daytime. The latent heat flux difference seems not to contribute to the daytime UCI in the case of the relatively moist soil conditions in the city.

Although the soil/surface parameters used in the current study (thermal inertia and moisture availability) are bulk parameters, as they do not account for vertical variations of soil moisture and its impacts on the bulk soil density, conductivity, and specific heat parameters required as input in mesoscale models, but they do account for the horizontal variations associated with complex land use patterns. Moisture availability has direct application in models not solving for the vertical distribution of soil moisture. For those models that do solve for this parameter, for example, MMS, RAMS, and URBMET/TVM, it can be used to provide the upper-boundary condition for the required initial vertical soil moisture profiles. Thermal inertia has direct application in models that do not solve for the vertical distribution of soil temperature. For those models that do solve for this parameter, it can be used to provide the hard-to-determine values of thermal diffusivity from the more easily obtained values of density and specific heat.

A natural extension of the current effort is the expanded utilization of remote sensing technique with models that do solve for soil moisture and to provide vegetative index (like NVDI) values in their vegetative cover modules. Another natural extension of the current effort is the application of the developed techniques to cases with a wider range of rural soil moisture content. This should be done in order to determine values for individual cities at which rural soils become moist enough so that their thermal inertia values become greater than that of their adjacent cities. Finally, methods need to be developed to remove the effects of the urban aerosol plume from satellite-derived spatial distributions of the surface/soil parameters required in mesoscale models.

Acknowledgments. This study is based in part on Jan Hafner's Ph.D. dissertation at the University of Alabama in Huntsville. The authors wish to thank Drs. Toby N. Carlson and Robert D. Bornstein for helpful discussion and suggestions. Dr. J. L. Aaron Song is thanked for his help with model runs. This research was funded by the U.S. Department of Energy's National Institute for Global Environmental Change (NIGEC) through the Southeast Regional Center at the University of Alabama-Tuscaloosa (DOE Cooperative Agreement DE-FC03-90ER61010). (Financial support does not constitute an endorsement by DOE of the views expressed in this work.) The Czech Academy of Science and the National Aeronautics and Space Administration (Grant NAS8-97082) are acknowledged for supporting the preparation and publication of the manuscript.

REFERENCES

- Aase, J. K., and S. B. Idso, 1975: Solar radiation interactions with mixed prairie rangeland in natural and denuded conditions. *Arch. Meteor., Geophys. Bioklimatol.*, **23B**, 255–264.
- Bornstein, R. D., 1975: The two-dimensional URBMET urban-boundary layer model. *J. Appl. Meteor.*, **14**, 1459–1477.
- , P. Thunis, and G. Schayes, 1993: Simulation of urban barrier effects on polluted urban boundary layers using three-dimensional URBMET/TVM model with urban topography. New results from NYC. *Air Pollution*, P. Zannetti et al., Eds., Computational Mechanics Publications, 15–34.
- Carlson, T. N., J. K. Dodd, S. G. Benjamin, and J. N. Cooper, 1981: Satellite estimation of the surface energy balance, moisture availability, and thermal inertia. *J. Appl. Meteor.*, **20**, 67–87.
- Changnon, S. A., 1992: Inadvertent weather modification in urban areas: Lessons for global climate change. *Bull. Amer. Meteor. Soc.*, **73**, 619–627.
- Dudhia, J., 1993: A nonhydrostatic version of the Penn State-NCAR Mesoscale Model: Validation tests and simulation of an Atlantic cyclone and cold front. *Mon. Wea. Rev.*, **121**, 1493–1513.
- Feng, J. Z., and D. E. Petzold, 1988: Temperature trends through urbanization in metropolitan Washington, D.C., 1945–1979. *Meteor. Atmos. Phys.*, **38**, 195–201.
- Gillies, R. R., and T. N. Carlson, 1995: Thermal remote sensing of surface soil water content with partial vegetation cover for incorporation into climate models. *J. Appl. Meteor.*, **34**, 745–756.
- Hirsave, P. P., R. M. Narayanan, B. T. Tracy, B. L. Gwilliam, R. L. Bolus, T. Pangburn, and H. L. McKim, 1996: Comparison of spatial statistics of SAR-derived and in-situ soil moisture estimates. *Proc. Remote Sensing for Sustainable Future, 1996 Int. Geoscience and Remote Sensing Symp.*, Lincoln, NE, IEEE Geoscience and Remote Sensing Society, 1073–1075.
- Hjelmfelt, M. R., 1982: Numerical simulation of the effects of St. Louis on mesoscale boundary layer airflow and vertical air motion: Simulation of urban versus nonurban effects. *J. Appl. Meteor.*, **21**, 1239–1258.
- Howard, L., 1833a: *Climate of London Deduced from Meteorological Observations*. 3d ed. Vol. 1. Harvey and Darton, 348 pp.
- , 1833b: *Climate of London Deduced from Meteorological Observations*. 3d ed. Vol. 2. Harvey and Darton, 407 pp.
- , 1833c: *Climate of London Deduced from Meteorological Observations*. 3d ed. Vol. 3. Harvey and Darton, 383 pp.
- Idso, S. B., R. D. Jackson, R. J. Reginato, B. A. Kimball, and F. S. Nakayama, 1975: The dependence of bare soil albedo on soil water content. *J. Appl. Meteor.*, **14**, 109–113.
- Jackson, T. J., and Coauthors, 1992: Multifrequency passive microwave observations of soil moisture in an arid rangeland environment. *Int. J. Remote Sens.*, **13**, 573–580.
- Johnson, G. T., T. R. Oke, T. J. Lyons, D. G. Steyn, I. D. Watson, and J. A. Voogt, 1991: Simulation of surface urban heat islands under “ideal” conditions at night. Part 1: Theory and tests against field data. *Bound.-Layer Meteor.*, **56**, 275–294.
- Karl, T. R., and P. D. Jones, 1989: Urban bias in area-averaged surface air temperature trends. *Bull. Amer. Meteor. Soc.*, **70**, 265–270.
- , H. F. Diaz, and G. Kukla, 1988: Urbanization: Its detection and effect in the United States climate record. *J. Climate*, **1**, 1099–1123.
- Kidwell, K. B., 1995: NOAA Polar Orbiter data user's guide. NOAA/NESDIS, Washington, DC, 410 pp. [Available online at <http://www2.ncdc.noaa.gov/POD/>.]
- Kustas, W. P., and Coauthors, 1991: An interdisciplinary field study of the energy and water fluxes in the atmosphere-biosphere system over semiarid rangelands: Description and some preliminary results. *Bull. Amer. Meteor. Soc.*, **72**, 1683–1705.
- , T. J. Schimugge, K. S. Humes, T. J. Jackson, R. Parry, M. A. Weltz, and M. S. Moran, 1993: Relationship between evaporative fraction and remotely sensed vegetation index and microwave brightness temperature for semiarid rangelands. *J. Appl. Meteor.*, **32**, 1781–1790.
- Manley, G., 1958: On the frequency of snowfall in metropolitan England. *Quart. J. Roy. Meteor. Soc.*, **84**, 70–72.
- McMillin, L. M., and D. S. Crosby, 1984: Theory and validation of the multiple window sea surface temperature technique. *J. Geophys. Res.*, **89**, 3655–3661.
- Moran, M. S., 1990: A window-based technique for combining Landsat Thematic Mapper thermal data with higher-resolution multispectral data over agricultural lands. *Photogramm. Eng. Remote Sens.*, **56**, 337–342.
- Myrup, L. O., 1969: A numerical model of the urban heat island. *J. Appl. Meteor.*, **8**, 908–918.
- O'Brien, J. J., 1970: A note on the vertical structure of the eddy exchange coefficient in the planetary boundary layer. *J. Atmos. Sci.*, **27**, 1213–1215.
- Oke, T. R., 1982: The energetic basis of the urban heat island. *Quart. J. Roy. Meteor. Soc.*, **108**, 1–24.
- , G. T. Johnson, D. G. Steyn, and I. D. Watson, 1991: Simulation of surface urban heat islands under “ideal” conditions at night. Part 2: Diagnosis of causation. *Bound.-Layer Meteor.*, **56**, 339–358.
- Ottle, C., and D. Vidal-Madjar, 1994: Assimilation of soil moisture inferred from infrared remote sensing in a hydrological model over the HAPEX-MOBILHY region. *J. Hydrol.*, **158**, 241–264.
- Pielke, R. A., 1974: A three-dimensional numerical model of the sea breezes over South Florida. *Mon. Wea. Rev.*, **102**, 115–139.
- , 1984: *Mesoscale Meteorological Modeling*. Academic Press, 612 pp.
- Price, J. C., 1979: Assessment of the urban heat island effect through the use of satellite data. *Mon. Wea. Rev.*, **107**, 1554–1557.
- Sailor, D. J., 1995: Simulated urban response to modifications in surface albedo and vegetative cover. *J. Appl. Meteor.*, **34**, 1694–1704.
- Schayes, G., and P. Thunis, 1990: A three-dimensional mesoscale model in vorticity mode. Contribution No. 60, Institut d'Astronomie et de Géophysique, Université Catholique de Louvain-la-Neuve, 42 pp. [Available from Université Catholique de Louvain, Institut d'Astronomie et de Géophysique, Georges Lemaitre, Chemin du Cyclotron 2, B-1348 Louvain-la-Neuve, Belgique.]
- , —, and R. Bornstein, 1996: Topographic vorticity mode mesoscale- β (TVM) model. Part I: Formulation. *J. Appl. Meteor.*, **35**, 1815–1823.
- Sellers, W. D., 1969: A global climatic model based on the energy balance of the earth-atmosphere system. *J. Appl. Meteor.*, **8**, 391–400.

- Stull, R. B., 1988: *An Introduction to Boundary Layer Meteorology*. Kluwer Academic, 666 pp.
- Swaid, H., 1993: The role of radiative-convective interaction in creating the microclimate of urban street canyons. *Bound.-Layer Meteor.*, **64**, 231-259.
- Taha, H., 1996: Modeling impacts of increased urban vegetation on ozone air quality in the South Coast Air Basin. *Atmos. Environ.*, **30**, 3423-3430.
- , 1997: Modeling the impacts of large-scale albedo changes on ozone air quality in the South Coast Air Basin. *Atmos. Environ.*, **31**, 1667-1676.
- Tapper, N. J., P. D. Tyson, I. F. Owens, and W. J. Hastie, 1981: Modeling the winter urban heat island over Christchurch, New Zealand. *J. Appl. Meteor.*, **20**, 365-376.
- Thunis, P., and R. Bornstein, 1996: Hierarchy of mesoscale flow assumptions and equations. *J. Atmos. Sci.*, **53**, 380-397.
- Tripoli, G. J., and W. R. Cotton, 1982: The Colorado State University three-dimensional cloud/mesoscale model—1982. Part I: General theoretical framework and sensitivity experiments. *J. Rech. Atmos.*, **3**, 185-219.
- Troufleau, D., A. Vidal, A. Beaudoin, M. S. Moran, M. A. Weltz, D. C. Goodrich, J. Washburn, and A. F. Rahman, 1994: Using optical-microwave synergy for estimating surface energy fluxes over semi-arid rangeland. *Proc. 6th Int. Symp. on Physical Measurements and Signatures in Remote Sensing*, Val d'Isere, France, Centre Nationale d'Études Spatiales, 1167-1174.
- Vukovich, F. M., J. W. Dunn III, and B. W. Crissman, 1976: A theoretical study of the St. Louis heat island: The wind and temperature distribution. *J. Appl. Meteor.*, **15**, 417-440.
- Wetzel, P. J., D. Atlas, and R. H. Woodward, 1984: Determining soil moisture from geosynchronous satellite infrared data: A feasibility study. *J. Appl. Meteor.*, **23**, 375-391.
- Yoshikado, H., 1992: Numerical study of the daytime urban effect and its interaction with the sea breeze. *J. Appl. Meteor.*, **31**, 1146-1164.